



Article

# Electric Properties of Multiwalled Carbon Nanotubes Dispersed in Liquid Crystals and Their Influence on Freedericksz Transitions

Emil Petrescu <sup>†</sup> and Cristina Cirtoaje <sup>\*,†</sup>

Department of Physics, Faculty of Applied Science, University Politehnica of Bucharest, RO-060042 Bucharest, Romania; emil.petrescu@upb.ro

\* Correspondence: cristina.cirtoaje@upb.ro

† These authors contributed equally to this work.

**Abstract:** Liquid crystal composites with multiwalled carbon nanotubes present dielectric properties considerably different from those of pure liquid crystal (LC). Using a proper dispersion of nanotubes in the LC-sample and a theoretical model in agreement with the experimental configuration, the dielectric permittivities of multiwalled carbon nanotubes are calculated. The influence of dielectric properties on the Freedericksz transition threshold is discussed. Theoretical values for dielectric permittivities of multiwalled carbon nanotubes are calculated for different temperatures

**Keywords:** carbon nanotubes; nematic liquid crystals; Freedericksz transition; electric properties



**Citation:** Petrescu, E.; Cirtoaje, C. Electric Properties of Multiwalled Carbon Nanotubes Dispersed in Liquid Crystals and Their Influence on Freedericksz Transitions. *Nanomaterials* **2022**, *12*, 1119. <https://doi.org/10.3390/nano12071119>

Academic Editor: Zoltán Kónya

Received: 11 March 2022

Accepted: 25 March 2022

Published: 28 March 2022

**Publisher's Note:** MDPI stays neutral with regard to jurisdictional claims in published maps and institutional affiliations.



**Copyright:** © 2022 by the authors. Licensee MDPI, Basel, Switzerland. This article is an open access article distributed under the terms and conditions of the Creative Commons Attribution (CC BY) license (<https://creativecommons.org/licenses/by/4.0/>).

## 1. Introduction

Recently, an increased interest of scientists and engineers on nano- and micro-materials led to a fast development of new materials and devices. Any materials containing particles with less than 100 nm in diameter are considered nanomaterials and can be used as thin films or surface coatings, on computer chips, as nanowires, nanotubes, or as liquid dispersion of tiny nanocrystalline particles. In the beginning, nanoparticles were observed as naturally occurring elements in volcanic ash, as residual elements, or as emissions in the combustion process of power plant chimneys and diesel engines, and they were known as ultrafine particles. After the development of the scanning tunneling microscope, nanomaterials were deliberately synthesized in different laboratories to improve the material's physical and chemical properties for a specific purpose or function. Carbon nanotubes (CNT) are some of the first discovered and synthesized nanomaterials [1–5]. They are also the most studied and used in various fields, from electronic and communication engineering [6–8] to chemistry [9,10], environmental science [11,12] and medicine [13,14]. Initially, experimental and theoretical studies were made on their physical properties such as magnetic properties [15–18], optical transmission and absorbency [19,20], electrical or thermal conductivity [21–23] and mechanical strength or elasticity [24]. More advanced theoretical models were proposed to provide a deeper understanding of phenomena in the nanoscale world including nanoparticles and/or liquid crystal molecules [25–31]. Although the applications might be various and probably will bring a considerable improvement to many systems, some suspicion appears as a result of incomplete knowledge of their physical properties [12], and information about toxic effects on devices functionality or even on life itself, which may be induced by ignorance. A serious problem when trying to study CNT's properties comes from organization. Isotropic powders or dispersion present randomly oriented nanotube axes and, thus, some properties may be strongly affected, leading to a behavior more similar to macroscopic bulk than nanoparticles ensemble. Without a proper alignment, especially for long particles such as nanotubes or nanowires, their true potential cannot be reached. A soft organized environment is needed. Liquid crystals

are good candidates because they seem to align their director with the nanotube’s long axis [32–35]. Starting from this point, we designed a theoretical model to describe the electro-optic behavior of carbon nanotubes dispersion in nematic liquid crystals at room temperature. The dielectric permittivities of carbon nanotubes were evaluated and their influence on Freedericksz transition threshold voltage of 7CB composite with multiwalled carbon nanotubes (MWCNT) was discussed.

### 2. Theory

When a low concentration of CNTs are inserted into a liquid crystal cell, the molecules tend to align themselves parallel to the nanotube’s long axis as represented in Figures 1 and 2. This alignment influences their orientation under an external field, and thus, the Freedericksz transition threshold voltage.

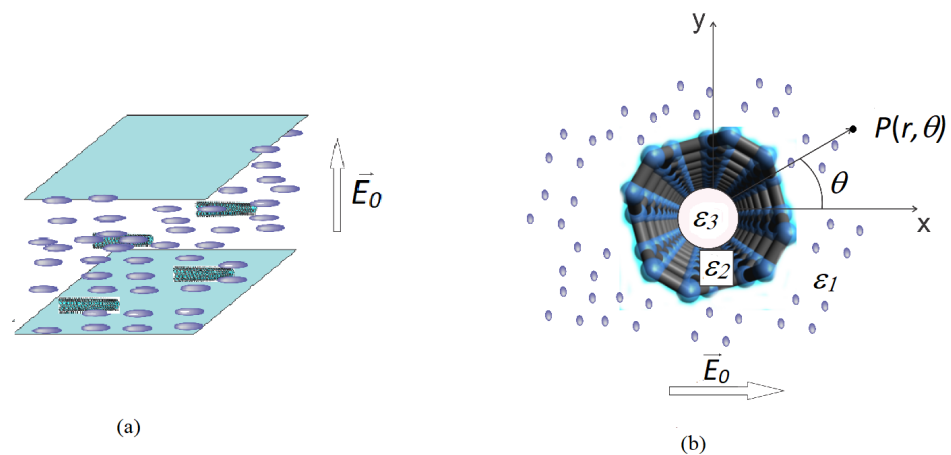


Figure 1. Planar cell containing LC+MWCNT composite: (a) the whole cell view, (b) inside view .

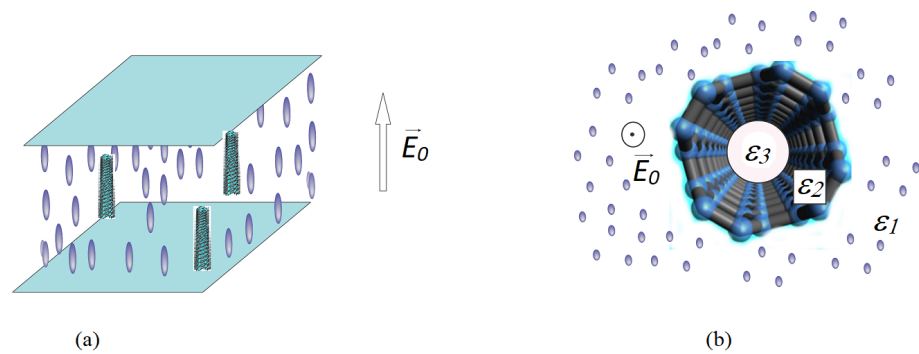


Figure 2. Homeotropic cell containing LC + MWCNT composite. (a) the whole cell view, (b) inside view.

As presented in [36] the threshold voltage can be evaluated by:

$$U = U_0 \sqrt{\frac{\epsilon_a}{\epsilon_{a\text{eff}}} \left( 1 - \frac{4\tau w f L^2}{\pi^2 K_1 a} \right)} \tag{1}$$

There are several factors that can affect the transition. One of them is the temperature which affects the Frank elastic constant  $K_1$  and induces a decrease in the threshold voltage on a specific range where the order is reasonably maintained [37,38]:

$$K_i = K_{i0} \left( 1 - \frac{T}{T_c} \right)^{2\beta} \tag{2}$$

The coefficient  $i$  refers to the order of the elastic constant ( $i = 1, 2, 3$  for splay, twist and bend elastic deformation),  $T$  is the absolute temperature of the sample,  $T_c$  is the clearing

temperature of the liquid crystal,  $\beta$  is a material constant [37] and  $K_{i0}$  are the elastic constants at  $T = 273.15$  K.

Another factor, is the anchoring energy density ( $w$ ) through the interaction process described by Burylov and Zakhlevnykh in [30]:

$$F(w, f) = \frac{4wfL^2}{\pi^2 K_1 a} \quad (3)$$

where  $w$  is the anchoring energy density,  $f$  is the volumetric fraction of nanotubes,  $L$  is the cell's thickness,  $K_1$  is the splay elastic constant and  $a$  is the nanotube outer radius.

Finally there is the dielectric anisotropy of the composite  $\varepsilon_{a\text{eff}}$  which can be controlled by the amount of carbon nanotubes inserted into the sample. This can be performed with a precise knowledge of the nanotube's permittivity and of the microscopic processes involved in the sample's configuration. For the carbon nanotube's dispersion in planar aligned cell, (Figure 1) we consider a physical system of an empty semiconductor cylinder in a dielectric environment. This system is in agreement with the experiment because, the liquid crystal, which is quite viscous, will not enter inside the narrow tube. If an external electric field  $E_0$  is applied to the LC cell, its direction will be perpendicular to the molecular direction and to the nanotube's axis as shown in Figure 1b. Due to the polarization effects, the effective field inside sample ( $E$ ), can be calculated as an average field on a large domain of the mixture. According to this domain, the mixture behaves like a homogeneous environment described by electric displacement  $D$ . By integrating the entire cell volume we obtain:

$$\frac{1}{V} \int_V (D - \varepsilon_1 \varepsilon_0 E) dv = \bar{D} - \varepsilon_1 \varepsilon_0 \bar{E} \quad (4)$$

where  $V$  is the mixture's volume,  $\varepsilon_0$  is the vacuum electric permittivity and  $\varepsilon_1$  is the dielectric constant of LC.  $\bar{E}$  and  $\bar{D}$  are the average field parameters in the mixture. The integral covers a succession of three regions with different permittivities as shown in Figure 1b: the first one is the air inside the tube with the dielectric permittivity  $\varepsilon_0$ , the second one is the nanotube's wall with the permittivity  $\varepsilon_2$  and the third one is the liquid crystal surrounding the tube with the permittivity  $\varepsilon_1$  so Equation (4) becomes:

$$\frac{1}{V} \int_{ext}^a (D_1 - \varepsilon_1 \varepsilon_0 E_1) dv + \frac{N}{V} \int_0^b (D_3 - \varepsilon_1 \varepsilon_0 E_3) 2\pi r l dr + \frac{N}{V} \int_b^a (D_2 - \varepsilon_1 \varepsilon_0 E_2) 2\pi r l dr = \bar{D} - \varepsilon_1 \varepsilon_0 \bar{E} \quad (5)$$

where  $l$  is the nanotube length and  $N$  is the nanotubes number in the mixture,  $D_1 = \varepsilon_1 \varepsilon_0 E_1$  is the electric displacement around CNT in LC,  $D_2 = \varepsilon_2 \varepsilon_0 E_2$  is the electric displacement inside the nanotube wall and  $D_3 = \varepsilon_3 \varepsilon_0 E_3 = \varepsilon_0 E_3$  is the electric displacement inside the tube (Figure 1),  $a$  is the outer radius of the tube and  $b$  is its inner radius.

It can be easily observed that the first integral is null because  $D_1 = \varepsilon_1 \varepsilon_0 E_1$ , so we only have two integrals:

$$I_2 = \int_b^a (D_2 - \varepsilon_1 \varepsilon_0 E_2) 2\pi r l dr \quad (6)$$

$$I_3 = \int_0^b (D_3 - \varepsilon_1 \varepsilon_0 E_3) 2\pi r l dr \quad (7)$$

Using the electrostatic principles of the dielectrics described by Landau and Lifsit in [39], we can calculate the integral using the electric field in each region from the electric potential

of the applied field in a point P determined by cylindrical coordinates  $r$  and  $\theta$ . For a point situated outside the nanotube the potential is:

$$\varphi_1 = -E_0 \cos \theta \left( r - \frac{A}{r} \right) \quad r > a, \quad (8)$$

for a point situated inside the nanotube's wall we obtain:

$$\varphi_2 = -CE_0 \cos \theta \left( r - \frac{G}{r} \right) \quad b \leq r \leq a \quad (9)$$

and for a point inside the CNT it results:

$$\varphi_3 = -E_0 r B \cos \theta \quad (10)$$

where  $A$ ,  $B$ ,  $C$  and  $G$  are constants and can be determined from the boundary conditions of each region from which we obtain:

$$\begin{aligned} \varphi_1(a) &= \varphi_2(a) \\ \varphi_2(b) &= \varphi_3(b) \\ \varepsilon_1 \varepsilon_0 \frac{\partial \varphi_1}{\partial r} \Big|_{r=a} &= \varepsilon_2 \varepsilon_0 \frac{\partial \varphi_2}{\partial r} \Big|_{r=a} \\ \varepsilon_2 \varepsilon_0 \frac{\partial \varphi_1}{\partial r} \Big|_{r=b} &= \varepsilon_0 \frac{\partial \varphi_3}{\partial r} \Big|_{r=b} \end{aligned} \quad (11)$$

Finally it results:

$$B = \frac{2}{\left(1 + \frac{\varepsilon_2}{\varepsilon_1}\right) - \frac{\varepsilon_2 - 1}{\varepsilon_2 + 1} \left(\frac{\varepsilon_2}{\varepsilon_1} - 1\right) \frac{b^2}{a^2}} \left(1 + \frac{\varepsilon_2 - 1}{\varepsilon_2 + 1}\right) \quad (12)$$

$$G = -\frac{(\varepsilon_2 - 1)}{(\varepsilon_2 + 1)} b^2 \quad (13)$$

$$C = \frac{2}{\left(1 + \frac{\varepsilon_2}{\varepsilon_1}\right) - \frac{\varepsilon_2 - 1}{\varepsilon_2 + 1} \left(\frac{\varepsilon_2}{\varepsilon_1} - 1\right) \frac{b^2}{a^2}} \quad (14)$$

Considering the external field  $E_0$  parallel to  $Ox$  axis, we have  $x = r \cos \theta$  and we obtain:

$$E_2 = -\frac{\partial \varphi_2}{\partial x} = CE_0 \left[1 + \frac{G}{r^2}\right] \quad (15)$$

and

$$E_3 = BE_0 \quad (16)$$

Using Equations (15) and (16) in Equations (6) and (7) we obtain:

$$I_2 = \pi a^2 l \varepsilon_0 I_{02} E_0 \quad (17)$$

$$I_3 = \pi a^2 l \varepsilon_0 I_{03} E_0 \quad (18)$$

where

$$I_{02} = \frac{2(\varepsilon_2 - \varepsilon_1)}{\left(1 + \frac{\varepsilon_2}{\varepsilon_1}\right) - \frac{\varepsilon_2 - 1}{\varepsilon_2 + 1} \left(\frac{\varepsilon_2}{\varepsilon_1} - 1\right) \frac{b^2}{a^2}} \left[ \left(1 - \frac{b^2}{a^2}\right) - \frac{\varepsilon_2 - 1}{\varepsilon_2 + 1} \frac{b^2}{a^2} \ln \frac{a}{b} \right] \quad (19)$$

$$I_{03} = \frac{2(1 - \varepsilon_1)}{\left(1 + \frac{\varepsilon_2}{\varepsilon_1}\right) - \frac{\varepsilon_2 - 1}{\varepsilon_2 + 1} \left(\frac{\varepsilon_2}{\varepsilon_1} - 1\right) \frac{b^2}{a^2}} \left(1 + \frac{\varepsilon_2 - 1}{\varepsilon_2 + 1}\right) \frac{b^2}{a^2} \quad (20)$$

By denoting  $v = \pi a^2 l$  the volume of a single nanotube, Equation (5) becomes:

$$\frac{Nv}{V}\epsilon_0 E_0 [I_{02} + I_{03}] = \bar{D} - \epsilon_1 \epsilon_0 \bar{E} \quad (21)$$

Considering the applied field  $E_0$  is equal to the average field inside the mixture  $\bar{E}$  and replacing  $\bar{D} = \epsilon_{eff} \epsilon_0 \bar{E}$ , we obtain:

$$\epsilon_{eff} = \epsilon_1 + f(I_{02} + I_{03}) \quad (22)$$

where  $f = \frac{Nv}{V}$  is the volumetric fraction of carbon nanotubes in the mixture.

In this case, the field is perpendicular to the nanotube axis, and the nanotubes are parallel to the molecular director, so  $\epsilon_1 \equiv \epsilon_{\perp LC}$  and  $\epsilon_2 \equiv \epsilon_{\perp CNT}$ . Thus, we obtain:

$$\begin{aligned} \epsilon_{\perp eff} = \epsilon_{\perp LC} + & \frac{2f(\epsilon_2 - \epsilon_1)}{\left(1 + \frac{\epsilon_2}{\epsilon_1}\right) - \frac{\epsilon_2 - 1}{\epsilon_2 + 1} \left(\frac{\epsilon_2}{\epsilon_1} - 1\right) \frac{b^2}{a^2}} \left[ \left(1 - \frac{b^2}{a^2}\right) - \frac{\epsilon_2 - 1}{\epsilon_2 + 1} \frac{b^2}{a^2} \ln \frac{a}{b} \right] \\ & + \frac{2f(1 - \epsilon_1)}{\left(1 + \frac{\epsilon_2}{\epsilon_1}\right) - \frac{\epsilon_2 - 1}{\epsilon_2 + 1} \left(\frac{\epsilon_2}{\epsilon_1} - 1\right) \frac{b^2}{a^2}} \left(1 + \frac{\epsilon_2 - 1}{\epsilon_2 + 1}\right) \frac{b^2}{a^2} \end{aligned} \quad (23)$$

In expressions of  $I_{02}$  and  $I_{03}$  we also have  $\epsilon_1 \equiv \epsilon_{\perp LC}$  and  $\epsilon_2 \equiv \epsilon_{\perp CNT}$ .

The parallel component of the mixture's electric permittivity can be calculated in a similar way considering a homeotropic cell where the field director is parallel to the nanotube's axis as it is shown in Figure 1. In this case, we obtained:

$$\epsilon_{\parallel eff} = \epsilon_{\parallel LC} \left\{ 1 + f \left[ \left(1 - \frac{\epsilon_{\parallel CNT}}{\epsilon_{\parallel LC}}\right) \frac{b^2 - a^2}{a^2} + \left(1 - \epsilon_{\parallel LC}\right) \frac{b^2}{a^2} \right] \right\} \quad (24)$$

Using Equations (23) and (24) we can evaluate the dielectric anisotropy:

$$\epsilon_{a eff} = \epsilon_{\parallel eff} - \epsilon_{\perp eff} \quad (25)$$

Equation (25) offers the possibility to evaluate the dielectric permittivities of carbon nanotubes and allows a control of the Fredericksz transition threshold.

### 3. Materials and Methods

Previous research on carbon nanotubes dispersed in liquid crystals, reported a decrease in transition threshold when carbon nanotubes were added. In order to reproduce this effect and obtain a consistent decrease in the transition voltage, we prepared two samples with higher concentrations to be used in experimental research [40–42]. The analyzed samples were prepared by mixing 7CB nematic with multiwalled carbon nanotubes with the average length of 10  $\mu\text{m}$  inner diameter of  $2b = 4.5$  nm and the outer diameter  $2a = 10$  nm. The nanotubes were dispersed in toluene and sonicated for several hours until a good dispersion was obtained. The solution was mixed with the nematic and placed in a laboratory clean room to evaporate the toluene. The mixture was weighed daily until the weight was constant and the evaporation process was finished. The resulted nanotubes concentrations were 0.36 wt% and 1.30 wt%. These mixtures were used to fill 15  $\mu\text{m}$  thick planar aligned cell from Instek and 15  $\mu\text{m}$  homeotropic cells prepared by us. Both types of cells have the effective area of 1  $\text{cm}^2$ . The Franck constants of 7CB were considered as given in [43] to be  $K_1 = 6.716 \times 10^{-12}$  N and  $K_2 = 3.674 \times 10^{-12}$  N.

The samples were analyzed by a polarized light microscope and it resulted that for high concentrations a clustering phenomena occurs leading to irregular micrometric structures as shown in Figure 3. The sample with a higher concentration of nanotubes presented an increase in the transition voltage due to agglomerations and due to different anchoring processes on microparticles formed inside the sample. For this structure of micrometric bulk dispersion, we cannot use the theoretical models presented in the previous section. For the lower concentration sample, the image is similar to the one obtained for the pure 7CB so the

molecular order is maintained and the nanotubes are well dispersed and aligned parallel to the nematic director as considered in the theory. For the 0.36% mass fraction of MWCNT with the nanotube powder concentration provided by the supplier ( $\rho = 0.07 \text{ g/cm}^3$ ), we obtained a volumetric fraction  $f = 6.5\%$ . In this case, we obtained a decrease in the Fredericksz transition as indicated in [40–42].

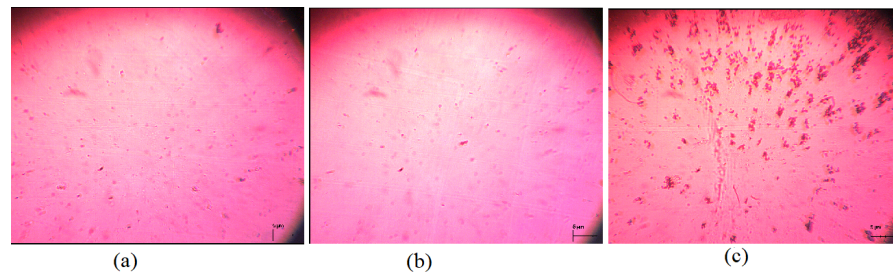


**Figure 3.** Polarized microscopy images recorded for planar aligned cells: (a) for 7CB sample, (b) for 7CB + 0.36% MWCNT and (c) for 7CB + 1.30% MWCNT

The measurements were performed on the set-up presented in Figure 4. A laser beam from the source was sent through the sample placed between two crossed polarizers. The polarizer's axes were set at  $45^\circ$  to the laser beam polarization direction to ensure the equal intensity for both ordinary and extraordinary rays. The emergent beam was recorded by a photovoltaic cell and the signal was sent to the computer. The power source used in the set-up has two functions: it can be used to apply a precise voltage on the sample at a set frequency but it can also record the capacity of the cell.

The nematic range was evaluated from the intensity versus temperature plot for each sample. The liquid crystal phase corresponds to the domain where significant intensity variation occurs due to the molecular reorientation induced by the laser beam (Figure 5). For the Fredericksz transition evaluation the capacity acquisition was switched off and the electric field applied was slowly increased by applying an alternate voltage (10 kHz) from the power source. The emergent beam intensity was determined for each voltage after a resting time of 2 s (much longer than the relaxation time of the mixtures to be sure that the systems is stabilized). The intensity versus applied voltage plots were recorded and the Fredericksz transition threshold was experimentally determined as the point where intensity starts the increase (Figure 6).

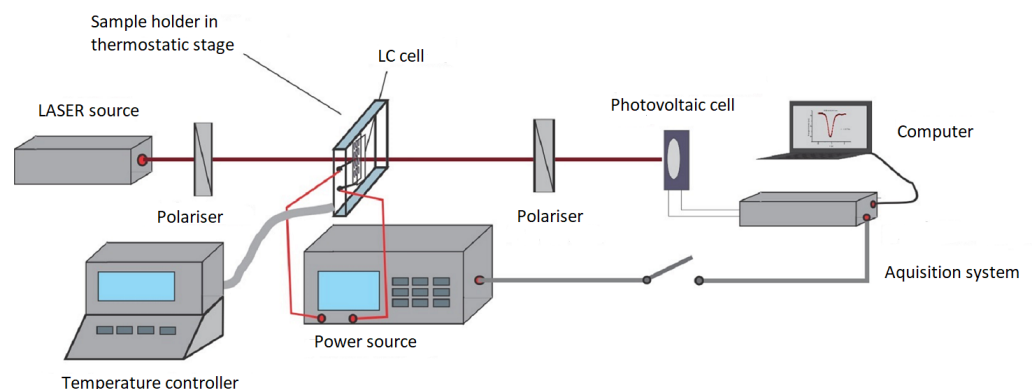


**Figure 4.** Experimental set-up for Fredericksz transition threshold.

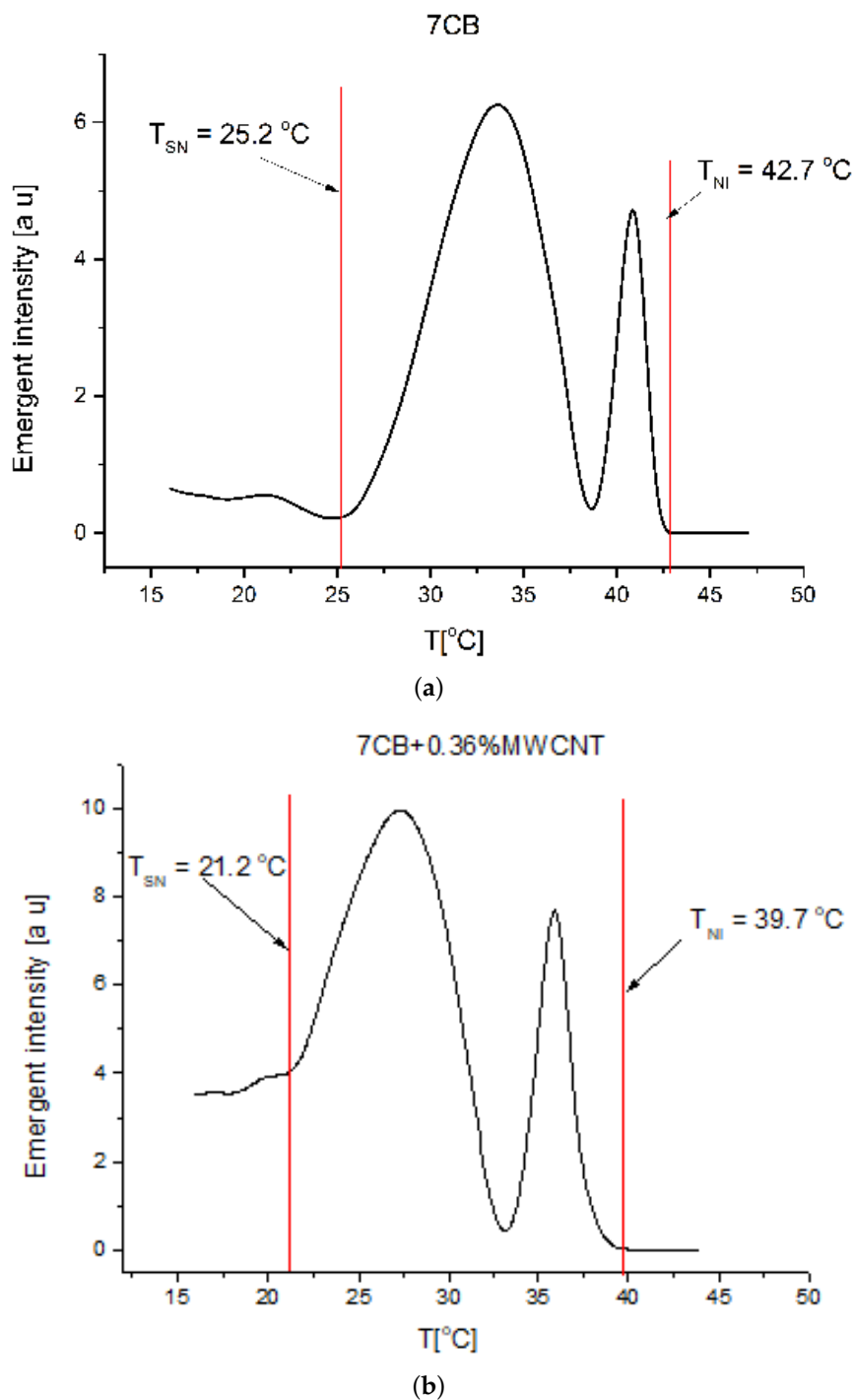
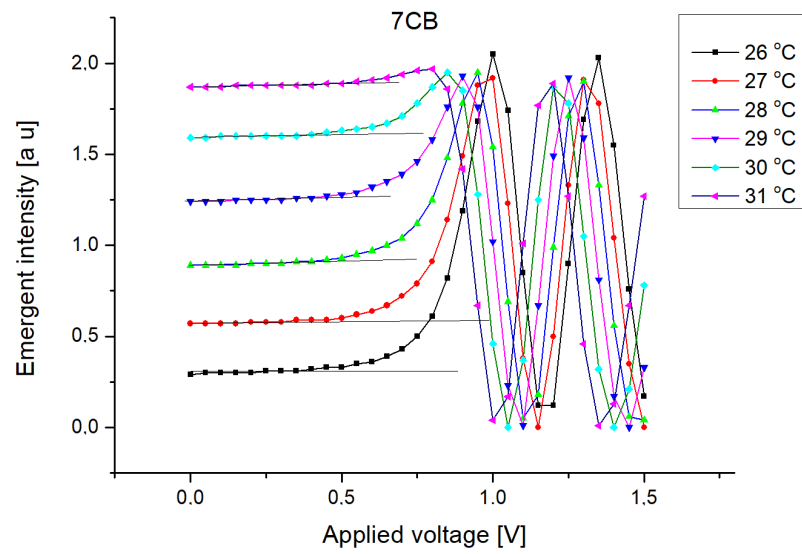
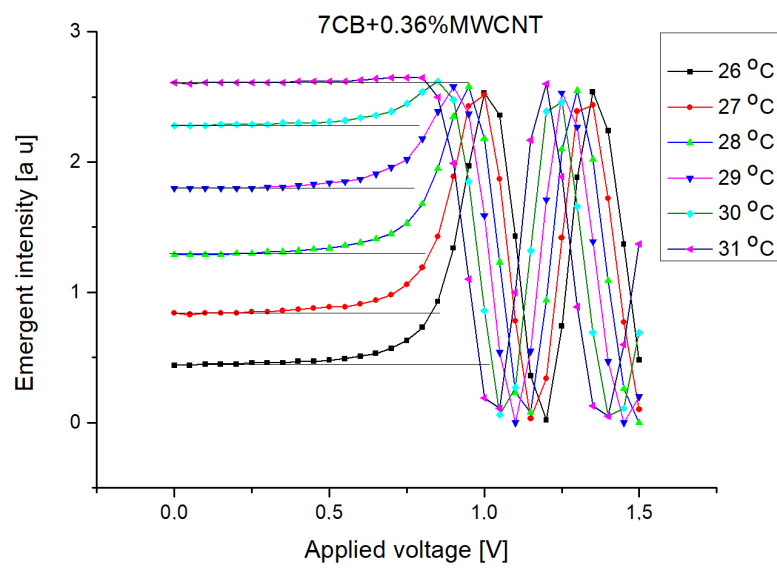


**Figure 5.** Emergent intensity versus temperature (a) for 7CB and (b) for 7CB + 0.36% MWCNT.

For the capacity measurements, the laser source was switched off and the acquisition system was enabled. The parallel capacitance was determined for the homeotropic cell and the perpendicular capacity was measured in the homogeneous aligned cell. The obtained values were adjusted by the capacitances of the empty cell. The dielectric permittivities were calculated from the capacitances by multiplying them with the thickness/active area ratio (the active area of each sample is 1 cm<sup>2</sup> and the thickness is 15 microns). The results are presented in (Figure 7). For the temperature depending plots, the LC cell was placed in the hot stage of a Mettler-Toledo thermo-stabilized heat source in which the temperature can be set by a precision of 0.01 degrees Celsius.



(a)



(b)

**Figure 6.** Emergent intensity versus applied voltage plots (a) for 7CB and (b) for 7CB + 0.36% MWCNT.

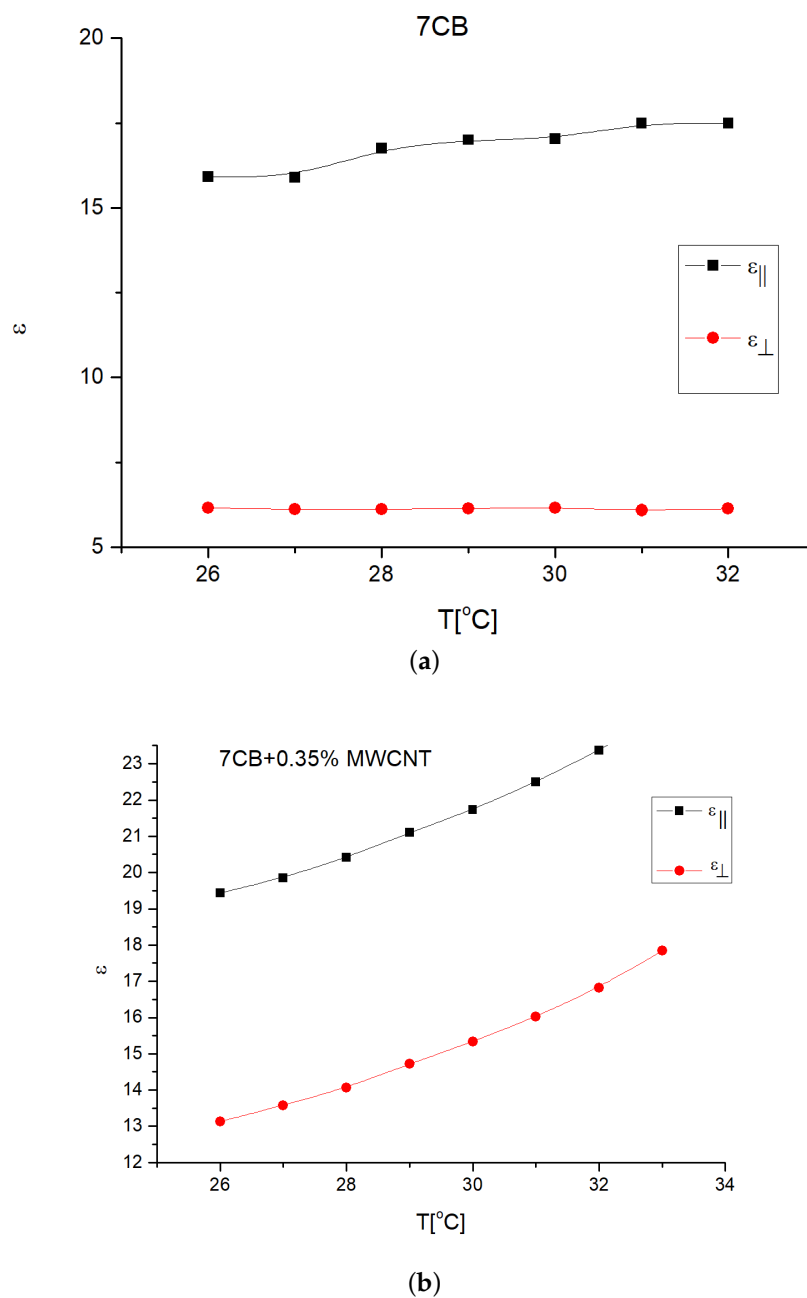


**Figure 7.** Parallel and perpendicular permittivities for (a) 7CB and (b) 7CB + 0.36% MWCNT.

#### 4. Results and Discussion

The Freedericksz transition voltage evaluated from Intensity versus Voltage plots given in Figure 6, and the dielectric anisotropy calculated from the permittivities given in Figure 7 are presented in Table 1. The temperature range was chosen in the first part of the nematic range of 7CB to keep the elastic constant variations very small around the average values of  $K_1 = 6.716 \times 10^{-12}$  N and  $K_2 = 36.74 \times 10^{-12}$  N in agreement with Equation (2) with a material constant of  $\beta = 0.1855$ .

As it can be observed, there is a considerable decrease (about 30%) in the threshold value for the sample containing multiwalled carbon nanotubes compared to the reference sample containing LC only. According to the formula given in Equation (1), this decrease may be explained by an increase in the effective anisotropy of the sample or by a variation of the anchoring energy of the molecules on the nanotube's surface. If we rewrite Equation (1) in a different form, we can use:

$$\frac{U}{U_0} = \sqrt{\frac{\epsilon_a}{\epsilon_{a\text{eff}}}} \sqrt{1 - F(w, f)} \tag{26}$$

where  $F(w, f) = \frac{4wfL^2}{\pi^2 K_1 a}$  is the anchoring depending term.

As it can be observed from Equation (26), we can decrease the threshold voltage  $U$  by increasing the anchoring energy or by increasing the nanotube’s anisotropy.

**Table 1.** Electric Freedericksz transition threshold for 7CB ( $U_0$ ) and for 7CB + MWCNTs ( $U$ ).

$T$ (°C)	$U_0$ [V]	$U$ [V]	$\epsilon_a$	$\epsilon_{a\text{eff}}$	$U_0/U$	$\sqrt{\epsilon_a \epsilon_{a\text{eff}}}$	$F(w, f)$
26	0.37	0.25	9.76	13.14	0.68	0.86	0.39
27	0.36	0.23	9.78	13.57	0.64	0.85	0.43
28	0.41	0.26	10.63	14.06	0.63	0.87	0.47
29	0.43	0.27	10.87	14.72	0.63	0.86	0.47
30	0.43	0.28	10.87	15.25	0.65	0.84	0.41
31	0.41	0.26	11.41	15.96	0.63	0.85	0.44

For our specific materials, the value of  $F(w, t)$  presented in Table 1 varies from 0.39 to 0.44 depending on the temperature but it can be adjusted by chemical functionalization of the nanotubes or by other chemical processes. A detailed discussion about this energy is provided in [35,36,39]. An increase in MWCNT concentration in the sample may also reduce the transition threshold but it must be performed with caution because it may induce the clustering effect as can be seen from Figure 3. Another way to decrease the threshold voltage is to increase the dielectric anisotropy by using other types of carbon nanotubes with different lengths and thicknesses.

Using Equations (23)–(25), we can calculate the parallel dielectric permittivity ( $\epsilon_{\parallel}$ ), the perpendicular permittivity ( $\epsilon_{\perp}$ ) and the dielectric anisotropy of carbon nanotubes ( $\epsilon_{a\text{CNT}}$ ). For the nanoparticles used in this experiment, the obtained permittivities are given in Table 2.

**Table 2.** Dielectric permittivities and anisotropy for MWCNT.

$T$ (°C)	$\epsilon_{\parallel\text{CNT}}$	$\epsilon_{\perp\text{CNT}}$	$\epsilon_{a\text{CNT}}$
26	42.66	15.11	27.55
27	44.84	16.21	28.67
28	45.85	20.45	25.46
29	48.36	21.30	27.09
30	50.98	30.16	20.77
31	53.53	41.30	12.23
32	57.18	49.37	7.81

It can be observed from the data obtained in Table 2 that MWCNT present a considerable higher dielectric anisotropy compared to the liquid crystals, and it may explain the composite reorientation at lower voltages and the decrease in the Freedericksz transition. It is also important to mention that, if the geometrical parameters of the nanotubes are known, the dielectric permittivities can be calculated if the effective anisotropy is known. Electro-optic applications, such as ultra-broadband electromagnetic wave absorption, Ref. [44] can benefit from the evaluation of parameters. An interesting aspect here is the temperature dependence of dielectric anisotropy. For the 7CB nematic, it increases with the temperature, while for nanotubes, we can notice it strongly decreases. Due to the small volumetric fraction of impurity the overall behavior is similar to the one of the liquid crystal but for the proper control of the transition threshold one must consider both dependencies.

## 5. Conclusions

This manuscript presents a discussion about the ways in which the carbon nanotubes inserted in the liquid crystal matrix can affect its dielectric properties. The nanotube content affects the average dielectric anisotropy and it can affect the temperature effect on Freedericksz transition. There are two possible applications of the aspects discussed in this article. The first one is from an engineering point of view: it can be used for the decrease in the transition threshold voltage by adjusting the amount of nanotubes or by using different coatings that may influence the anchoring strength or angle. This can be an advantage for LCDs because a lower transition voltage leads to a lower power consumption and a longer life for the batteries. From a scientific point of view, we proposed a theoretical method to determine the dielectric parallel and permittivity of carbon nanotubes. The liquid crystal environment is a proper tool to obtain an organized nanotubes ensemble as considered in the discussed theory. Thus, by simple measurements of LC cell capacity when filled with an LC+CNT composite, one can calculate the nanotube's permittivities.

**Author Contributions:** Conceptualization, E.P. and C.C.; methodology, C.C.; validation, E.P.; formal analysis, E.P.; investigation, C.C.; resources, E.P. and C.C.; data curation, C.C.; writing—original draft preparation, E.P.; writing—review and editing, E.P. and C.C.; visualization, C.C.; supervision, E.P.; project administration, C.C.; funding acquisition, C.C. All authors have read and agreed to the published version of the manuscript.

**Funding:** This research was funded by Romanian Governmental Representative at JINR Dubna, Grant no. 9/JINR order 365/11 May 2021: “Graphene nanoparticles dispersion in soft crystalline environment”.

**Data Availability Statement:** Not applicable.

**Conflicts of Interest:** The authors declare no conflict of interest.

## References

1. Saito, R.; Dresselhaus, G.; Dresselhaus, M.S. *Physical Properties of Carbon Nanotubes*; Imperial College Press: London, UK, 1998; ISBN 1-86094-093-5.
2. Harris, P.J.F. Carbon Nanotubes and Related Structures: New Materials for the Twenty-First Century. *Am. J. Phys.* **2004**, *72*, 415. [[CrossRef](#)]
3. Ajayan, P.M. Nanotubes from Carbon. *Chem. Rev.* **1999**, *99*, 1787–1799. [[CrossRef](#)]
4. Sinott, S.B.; Andrews, R. Carbon Nanotubes: Synthesis, Properties, and Application. *Crit. Rev. Solid. State. Mater. Sci.* **2001**, *26*, 145–249. [[CrossRef](#)]
5. Schoot, P.V.; Popa-Nita, V.; Kralj, S. Alignment of Carbon Nanotubes in Nematic Liquid Crystals. *J. Phys. Chem. B* **2008**, *112*, 4512–4518. [[CrossRef](#)]
6. Baughman, R.H.; Zakhidov, A.A.; de Heer, W.A. Carbon nanotubes—The route toward applications. *Science* **2002**, *297*, 787–792. [[CrossRef](#)] [[PubMed](#)]
7. Postma, H.W.C.; Teepen, T.; Yao, Z.; Grifoni, M.; Dekker, C. Carbon nanotube single-electron transistors at room temperature. *Science* **2001**, *293*, 76–79. [[CrossRef](#)] [[PubMed](#)]
8. Tseng, Y.C.; Xuan, P.Q.; Javey, A.; Malloy, R.; Wang, Q.; Bokor, J.; Dai, H. Monolithic Integration of Carbon Nanotube Devices with Silicon MOS Technology. *Nano Lett.* **2004**, *4*, 123–127. [[CrossRef](#)]
9. Zhang, M.; Fang, S.; Zakhidov, A.A.; Lee, S.B.; Aliev, A.E.; Williams, C.D.; Atkinson, K.R.; Baughman, R.H. Strong, transparent, multifunctional, carbon nanotube sheets. *Science* **2005**, *309*, 1215–1219. [[CrossRef](#)]
10. Dalton, A.B.; Collins, S.; Munoz, E.; Razal, J.M.; Ebron, V.H.; Ferraris, J.P.; Coleman, J.N.; Kim, B.G.; Baughman, R.H. Super-tough carbon-nanotube fibres. *Nature* **2003**, *423*, 703. [[CrossRef](#)]
11. Arico, A.S.; Bruce, P.; Scrosati, B.; Tarascon, J.M.; van Schalkwijk, W. Nanostructured materials for advanced energy conversion and storage devices. *Nat. Mater.* **2005**, *4*, 366–377. [[CrossRef](#)]
12. Das, R.; Leo, B.F.; Murphy, F. The Toxic Truth About Carbon Nanotubes in Water Purification: A Perspective View. *Nanoscale Res. Lett.* **2018**, *13*, 183. [[CrossRef](#)] [[PubMed](#)]
13. He, H.; Pham-Huy, L.A.; Dramou, P.; Xiao, D.; Zuo, P.; Pham-Huy, C. Carbon Nanotubes: Applications in Pharmacy and Medicine. *BioMed. Res. Int.* **2013**, *2013*, 578290. [[CrossRef](#)] [[PubMed](#)]
14. Zare, H.; Ahmadi, S.; Ghasemi, A.; Ghanbari, M.; Rabiee, N.; Bagherzadeh, M.; Karimi, M.; Webster, T.J.; Hamblin, M.R.; Mostafavi, E. Carbon Nanotubes: Smart Drug/Gene Delivery Carriers. *Int. J. Nanomed.* **2021**, *16*, 1681–1706. [[CrossRef](#)]
15. Cirtoaje, C.; Petrescu, E. Measurement of magnetic anisotropy of multiwalled carbon nanotubes in nematic. *Phys. E* **2016**, *84*, 244–248. [[CrossRef](#)]

16. Petrov, D.A.; Skokov, P.K.; Zakhlevnykh, A.N. Magnetic field induced orientational transitions in liquid crystals doped with carbon nanotubes. *Beilstein J. Nanotechnol.* **2017**, *8*, 2807–2817. [[CrossRef](#)] [[PubMed](#)]
17. Petrov, D.A.; Zakhlevnykh, A.N.; Mantsurov, A.V. Orientational Ordering of a Liquid-Crystal Suspension of Carbon Nanotubes in a Magnetic Field. *J. Exp. Theor. Phys.* **2018**, *127*, 357–369. [[CrossRef](#)]
18. Zakhlevnykh, A.N.; Petrov, D.A.; Skokov, P.K. Influence of Ferromagnetic Carbon Nanotubes on Magnetic Transitions in Liquid Crystals. *J. Exp. Theor. Phys.* **2018**, *127*, 767–777. [[CrossRef](#)]
19. Ara, M.H.M.; Dehghani, Z. Improvement of the third order nonlinear optical properties of nematic liquid crystal under the influence of different compositional percentage of doped SWCNT and the external electric field. *J. Mol. Liq.* **2019**, *275*, 281–289. [[CrossRef](#)]
20. Lisetski, L.N.; Minenko, S.S.; Fedoryako, A.P.; Lebovka, N.I. Dispersions of multiwalled carbon nanotubes in different nematic mesogens: The study of optical transmittance and electrical conductivity. *Phys. E* **2009**, *41*, 431–435. [[CrossRef](#)]
21. Koysal, O. Conductivity and dielectric properties of cholesteric liquid crystal doped with single wall carbon nanotube. *Synth. Met.* **2010**, *160*, 1097–1100. [[CrossRef](#)]
22. Jain, A.K.; Deshmukh, R.R. Electro-optical and dielectric study of multi-walled carbon nanotube doped polymer dispersed liquid crystal films. *Liq. Cryst.* **2019**, *46*, 1191–1202. [[CrossRef](#)]
23. Cirtoaje, C.; Petrescu, E.; Motoc, C. Electric field effects in nematic liquid crystals doped with carbon nanotubes. *Phys. E* **2013**, *54*, 242–246. [[CrossRef](#)]
24. Cetinkaya, M.C.; Yildiz, S.; Ozbek, H. The effect of -COOH functionalized carbon nanotube doping on electro-optical, thermo-optical and elastic properties of a highly polar smectic liquid crystal. *J. Mol. Liq.* **2018**, *272*, 801–814. [[CrossRef](#)]
25. Petrescu, E.; Cirtoaje, C. Dynamic behaviour of a nematic liquid crystal with added carbon nanotubes in an electric field. *Beilstein J. Nanotechnol.* **2018**, *9*, 233–241. [[CrossRef](#)] [[PubMed](#)]
26. Staic, M.D.; Petrescu-Nita, A. Symmetry group of two special types of carbon nanotube. *Acta Cryst.* **2013**, *A69*, 435–439. [[CrossRef](#)] [[PubMed](#)]
27. Petrescu, E.; Bena, R.E.; Cirtoaje, C. Polarization gratings using ferronematics—An elastic continuum theory. *JMMM* **2013**, *336*, 44–48. [[CrossRef](#)]
28. Cirtoaje, C.; Petrescu, E.; Stan, C.; Rogachev, A. Electric Fredericksz transition in nematic liquid crystals with graphene quantum dot mixture. *Appl. Surf. Sci.* **2019**, *487*, 1301–1306. [[CrossRef](#)]
29. Popa-Nita, V.; Kralj, S. Liquid crystal-carbon nanotubes mixtures. *J. Chem. Phys.* **2010**, *132*, 024902. [[CrossRef](#)]
30. Burylov, S.V.; Zakhlevnykh, A.N. Orientational energy of anisometric particles in liquid-crystalline suspensions. *Phys. Rev. E* **2013**, *88*, 012511. [[CrossRef](#)]
31. Petrov, D.A.; Zakhlevnykh, A.N. Statistical theory of magnetic field induced phase transitions in negative diamagnetic anisotropy liquid crystals doped with carbon nanotubes. *J. Mol. Cryst.* **2019**, *287*, 110901. [[CrossRef](#)]
32. Dierking, I.; Scalia, G.; Morales, P. Liquid crystal-carbon nanotube dispersions. *J. Appl. Phys.* **2005**, *97*, 044309. [[CrossRef](#)]
33. Dierking, I.; Scalia, G.; Morales, P.; LeClere, D. Aligning and reorienting carbon nanotubes with nematic liquid crystals. *Adv. Mater.* **2004**, *16*, 865–869. [[CrossRef](#)]
34. Chang, C.; Zhao, Y.; Liu, Y.; An, L. Liquid crystallinity of carbon nanotubes. *RSC Adv.* **2018**, *8*, 15780–15795. [[CrossRef](#)]
35. Yadav, S.P.; Singh, S. Carbon nanotube dispersion in nematic liquid crystals: An overview. *Prog. Mater. Sci.* **2016**, *80*, 38–76. [[CrossRef](#)]
36. Cirtoaje, C.; Petrescu, E.; Stoian, V. Electrical Fredericksz transitions in nematic liquid crystals containing ferroelectric nanoparticles. *Phys. E* **2015**, *67*, 23–27. [[CrossRef](#)]
37. Lin, S.; Y.Q. Temperature effect on threshold voltage and optical property of twisted nematic liquid crystal with applied different voltages. *Optik* **2010**, *121*, 1693–1697. [[CrossRef](#)]
38. Li, J.; Gauza, S.; Wu, S. Temperature effect on liquid crystal refractive indices. *J. Appl. Phys.* **2004**, *96*, 19–24. [[CrossRef](#)]
39. Landau, L.; Lifchitz, E. *Electrodynamique des Milieux Continues*; Editions MIR: Moscow, Russia, 1969.
40. Verma, R.; Mishra, M.; Dhar, R.; Dabrowski, R. Single walled carbon nanotubes persuaded optimization of the display parameters of a room temperature liquid crystal 4-pentyl-4'-cyanobiphenyl. *J. Mol. Liq.* **2016**, *221*, 190–196. [[CrossRef](#)]
41. Podgornov, F.V.; Suvorova, A.M.; Lapanik, A.V.; Haase, W. Electrooptic and dielectric properties of ferroelectric liquid crystal/single walled carbon nanotubes dispersions confined in thin cells. *Chem. Phys. Lett.* **2009**, *479*, 4–6. [[CrossRef](#)]
42. Singh, B.P.; Sikarwar, S.; Pandey, K.K.; Manohar, R.; Depriester, M.; Singh, D.P. Carbon Nanotubes Blended Nematic Liquid Crystal for Display and Electro-Optical Applications. *Electron. Mater.* **2021**, *2*, 466–481. [[CrossRef](#)]
43. Liu, P.; Jamieson, A. Twist viscosity of mixture of low molar mass nematics. *Rheol. Acta* **2000**, *39*, 532–541. [[CrossRef](#)]
44. Hou, T.; Jia, Z.; Dong, Y.; Liu, X.; Wu, G. Layered 3D structure derived from MXene/magnetic carbon nanotubes for ultra-broadband electromagnetic wave absorption. *Chem. Eng. J.* **2022**, *431*, 133919. [[CrossRef](#)]